An ultrafast terahertz probe of the transient evolution of the charged and neutral phase of photo-excited electron-hole gas in a monolayer semiconductor

2D Materials

PAPER

RECEIVED
14 September 2015

REVISED
15 November 2015

ACCEPTED FOR PUBLICATION
4 December 2015

PUBLISHED
18 January 2016

An ultrafast terahertz probe of the transient evolution of the charged and neutral phase of photo-excited electron-hole gas in a monolayer semiconductor

Xuefeng Liu[1,2], Hongyi Yu[3], Qingqing Ji[4], Zhihan Gao[1,2], Shaofeng Ge[1,2], Jun Qiu[1,2], Zhongfan Liu[4], Yanfeng Zhang[4,5] and Dong Sun[1,2]

[1] International Center for Quantum Materials, School of Physics, Peking University, Beijing 100871, People's Republic of China
[2] Collaborative Innovation Center of Quantum Matter, Beijing 100871, People's Republic of China
[3] Department of Physics and Center of Theoretical and Computational Physics, The University of Hong Kong, Hong Kong, People's Republic of China
[4] Center for Nanochemistry (CNC), Beijing National Laboratory for Molecular Sciences, College of Chemistry and Molecular Engineering, Academy for Advanced Interdisciplinary Studies, Peking University, Beijing 100871, People's Republic of China
[5] Department of Materials Science and Engineering, College of Engineering, Peking University, Beijing 100871, People's Republic of China

E-mail: sundong@pku.edu.cn

Keywords: transition-metal dichalcogenides, terahertz, ultrafast dynamics, dark exciton

Supplementary material for this article is available online

Abstract

We investigate the dynamical formation of an exciton from photo-excited electron-hole plasma and its subsequent decay dynamics in monolayer MoS_2 grown by chemical vapor deposition (CVD) using ultrafast pump and terahertz probe spectroscopy. Different photo-excited electron-hole states are resolved based on their distinct responses to THz photon and decay lifetimes. The observed transient THz transmission can be fitted with two decay components: a fast component with a decay lifetime of 20 ps, which is attributed to the exciton lifetime, including its formation and subsequent intra-exciton relaxation; a slow component with an extremely long decay lifetime of several ns, possibly due to a long-lived dark exciton state. The relaxation dynamics are further supported by temperature and pump-fluence-dependent studies of the decay time constants. The sign of the transient THz observed in this experiment is the opposite of that measured in a recent parallel transient THz work on MoS_2 [1]. The observed decay dynamics are also different, and the possible reasons for these discrepancies are discussed.

Introduction

Monolayer transition-metal dichalcogenides (TMDCs) as a new category of two dimensional (2D) materials, are of intense research interest in the post-graphene era due to their exceptional optoelectronic properties as 2D semiconductor counterparts of graphene [2–5], versatile capabilities regarding spin and valley pseudospin - quantum control through their Berry-phase-related properties, and strong spin–orbit coupling [6]. Central to governing these unique properties is the behavior of the charge carriers in 2D TMDC, which are subjected to substantial Coulomb interactions due to strong quantum confinement and reduced screening in the strict 2D limit. This leads the photo-excited electron-hole pairs to form an electron-hole bound state, known as an exciton, which dominates the optoelectronic response and serves as carrier of various quantum degrees of freedom in 2D TMDC [6]. A recent experiment has shown that the tightly bound exciton can further capture additional excess charges to form a trion (a charged exciton) [3, 7]. Compared to conventional bulk semiconductors, and with its low dimensional structure as a semiconductor quantum well [8], 2D TMDC processes very large amounts of binding energy up to a few hundred meV for an exciton [9–16] and high dissociation energies up to 50 meV for a trion [3, 7, 17]. These values are an order of magnitude larger than those of their multilayer and bulk crystal counterparts [18]. Due to the extremely large amount of binding energy, understanding the evolution dynamics of the neutral and charged phase from the optically excited

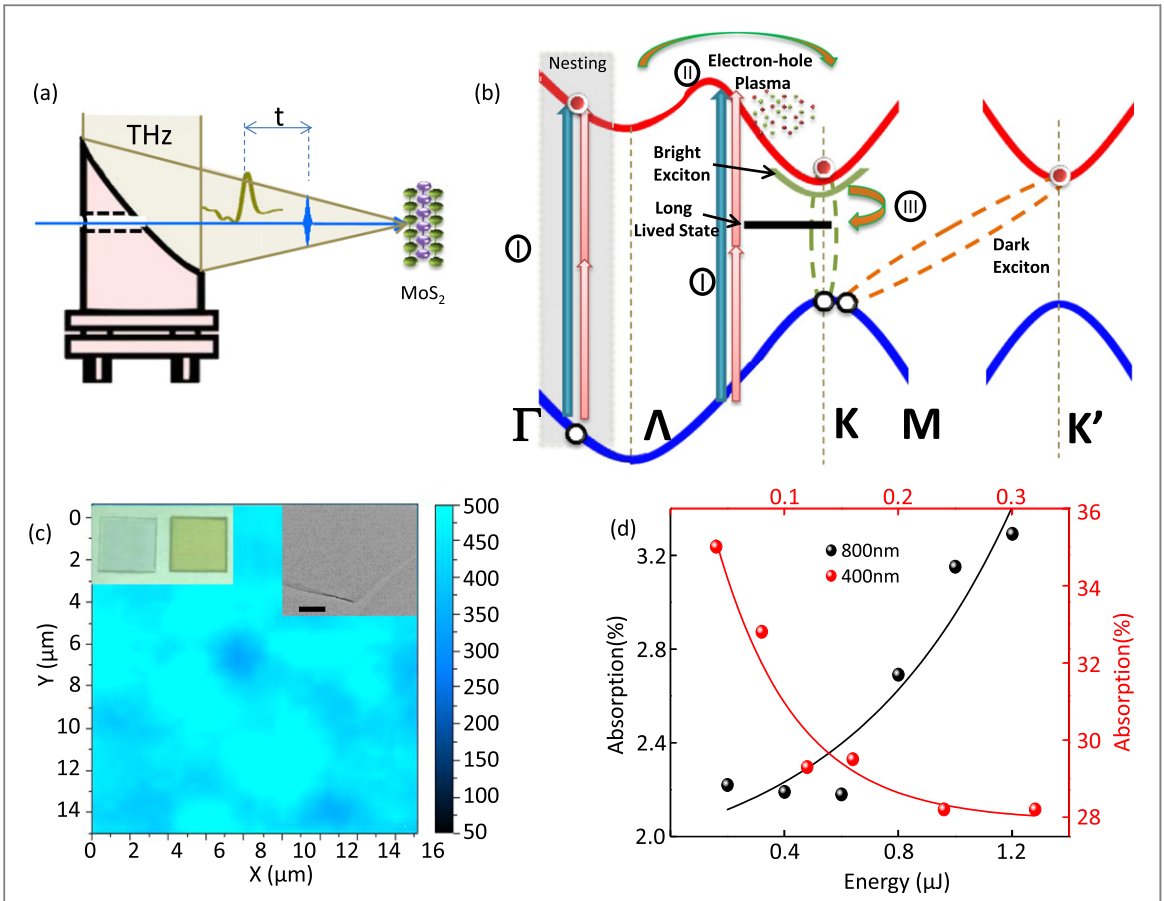

Figure 1. Ultrafast pump and terahertz probe spectroscopy on CVD-grown monolayer MoS_2. (a) Experimental setup. (b) Relaxation dynamics of the electron-hole plasma after one-photon or two-photon photo-excitation. (c) PL mapping at 670 nm of the MoS_2 sample with 532 nm CW excitation. The left inset is an optical image of a bare sapphire substrate (left) and a sapphire substrate covered by monolayer MoS_2 (right). The sample size is 10 mm × 10 mm × 0.5 mm. The right inset is a TEM image of the MoS_2 sample. The scale bar is 200 nm. (d) The absorption coefficient of the monolayer MoS_2 at different pulse energies.

eletron-hole plasma is an interesting topic which remains elusive in TMDCs—although it has been well studied in traditional semiconductors [19, 20].

Early efforts regarding carrier/exciton dynamics studies—especially the valley dynamics of MoS_2 and other transition-metal dichalcogenides—include studies with various ultrafast optical spectroscopy tools such as time-resolved photoluminescence spectroscopy [21, 22], transient reflection/transmission in the visible frequency range and the Kerr rotation experiment [23–32]. As a probe sensitive to the exciton state, the THz response not only shows contrast between charged photo-excited electron-hole plasma and the neutral exciton, but can also tell different species of exciton through their different responses in the THz range [22]. In this paper, we apply ultrafast pump and terahertz probe spectroscopy to a chemical-vapor-deposition-grown monolayer MoS_2 sample to study the exciton formation and evolution dynamics of photo-excited electron-hole plasma. Through the transient THz experiment, a long decay component (~ns) is observed, which indicates the existence of a long-lived exciton state. The schematic diagram of the experiment is shown in figure 1(a): 3.1 eV (400 nm) or 1.55 eV (800 nm) pump photons are used to excite the sample through direct one-photon or two-photon interband optical transition. The photon energy is sufficient to produce electron-hole plasma with above-bandgap excitation after intervalley relaxation to the K (K′) valley. After excitation, a terahertz pulse emitted at various pump-probe delay times, t, probes the following evolution starting from the electron-hole plasma by monitoring the pump- induced terahertz transmission change through the sample. Due to the different charge characters, effective masses and decay lifetimes, different states that evolve after photo-excitation, namely, electron-hole plasma, bright, dark or trapped excitons (figure 1(b)) have different responses to the THz field. Based on the differences in photo-excited states, the THz probe can then resolve them, which will be discussed later.

Methods

To perform terahertz time domain pump probe spectroscopy measurements, a 250 kHz Ti-sapphire amplifier (RegA) system [33] is employed to generate laser pulses of 800 nm (1.55 eV) and 60 fs. The laser was split into three beams: one beam is either directly

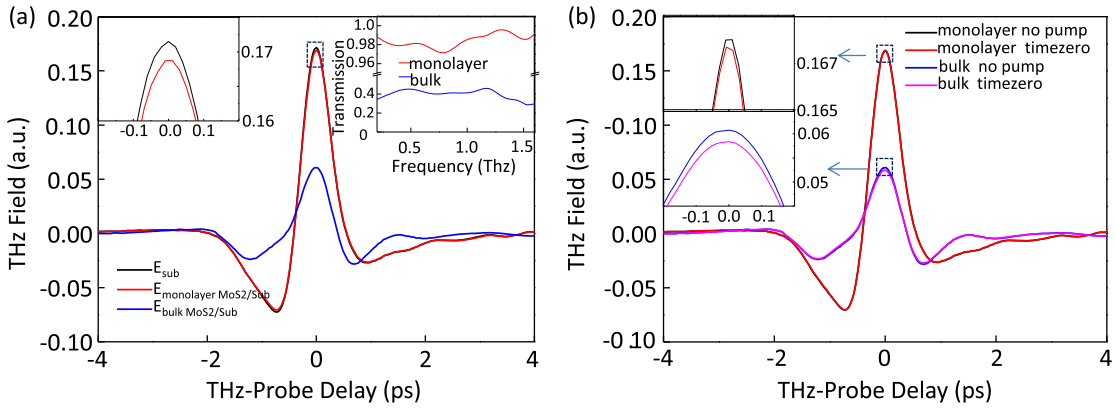

Figure 2. THz transmission of MoS_2. (a) THz transmission through the monolayer and bulk MoS_2 samples as well as the bare substrate in equilibrium condition. The left inset is a zoomed-in view of the terahertz field peak marked by a rectangle in the main figure. The right inset shows the transmission spectrum of monolayer and bulk MoS_2. (b) Pump-induced reduction of the THz transmission of monolayer and bulk MoS_2 at time zero. The pump light is 400 nm, and the excitation energy is 0.32 μJ. The two insets are zoomed-in views of the peak areas as marked by the rectangular area in the main figure.

used or frequency-doubled with a BBO crystal for the ultrafast pump; the second beam is used to generate THz through a GaAs photoconductive switch; the third beam is used to map out the THz electric field waveform in the time domain through a 1 mm thick ZnTe crystal using a standard electro-optic sampling technique [34]. The pump beam is mechanically chopped at 1.5 kHz and the probe THz is detected using a lock-in amplifier referred to as a chopper. The effective bandwidth of the sampling system is limited to 1.7 THz by phase-matching in the ZnTe crystal and absorption of the fused silica windows of the cryostat. In our measurement, the generated THz combined with the optical pump beam are co-linearly polarized and overlapped on the sample with a 1.5 mm and 2 mm (FWHM intensity) spot-size respectively.

The large-area monolayer MoS_2 samples are grown by chemical vapor deposition (CVD) on a sapphire substrate [35]. The fabrication detail of these CVD samples is provided in reference [35]. The left inset of figure 1(c) shows the color contrast of the sapphire substrate with and without the monolayer MoS_2 on it. The right inset of figure 1(c) shows the TEM image of the sample transferred onto copper grids, wherein an unintentional scratch is utilized to identify the monolayer nature of the film. The CVD sample we used has over a 96% monolayer coverage, as verified from the PL mapping in figure 1(c), showing a homogeneous intensity in the length scale of tens of microns. The electron doping density of a typical sample can be estimated from the transport measurement, which is less than 7×10^{11} cm^{-2}. The single crystal domain size is estimated to be around 2 μm, which is much smaller than the mm diameter THz spot. Due to the relatively large grain size, the fast tunneling transport through the grain boundary makes only a minor contribution to the THz response, which should not affect any of the relatively long dynamics (>2 ps) measured in this work [36]. For comparison, the same THz probe experiment is also performed on thick MoS_2 samples (>100 nm) exfoliated from natural minerals and transferred onto the sapphire substrate.

Results

The one-photon absorption rate of 400 nm is measured to be around 30% by comparing power transmission through MoS_2/sapphire and sapphire (figure 1(d)). This extremely large monolayer absorption is due to the band nesting effect in MoS_2, which has been discussed extensively in recent literature [37]. We note that reflection and scattering are ignored in the measurement, and that the transmission measurement thus slightly overestimates the absorption rate. With 0.32 μJ excitation energy, the absorption rate converts to a photo-excited electron hole density of 4.4×10^{12} cm^{-2}. For two-photon absorption of 800 nm, the measured absorption coefficient is below 2.3%, which converts to an electron-hole density of 5×10^{11} cm^{-2}. Figure 2(a) shows a typical terahertz field waveform through a bare substrate, monolayer MoS_2 and bulk MoS_2 on sapphire. The monolayer MoS_2 shows about 2.3% absorption at the THz peak field. In the time-resolved measurement, we fix the THz sampling delay at the THz peak field and scan the pump-probe delay, t, between the infrared pump and THz probe. Figure 3(a) shows the temporal evolution of the fractional change of the THz field $\Delta E(t, 0)/ E(0)$, where $\Delta E(t, 0)$ is the pump-induced transmitted THz peak field change at the pump-probe delay, t, and E(0) is the transmitted THz peak field with no pump excitation. The rising time of the response is about 2 ps in the monolayer (figure 3(b)), which is attributed to scattering from the initial excited C band to the K (K′) valley. The rising time is reduced to 1.2 ps in the bulk, possibly due to the band structure difference. The pump fluence of 400 nm and 800 nm are both

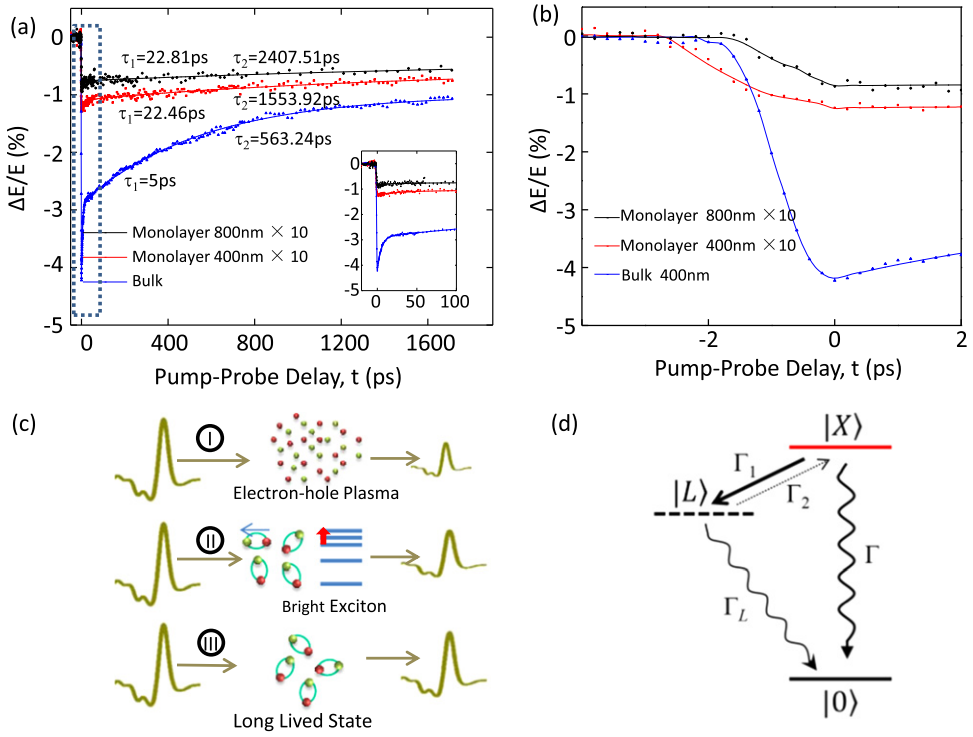

Figure 3. Transient THz response of MoS_2. (a) Temporal evolution of the transient terahertz responses of the monolayer and bulk MoS_2 with 400 nm and 800 nm excitation, experimental data (dots) and bi-exponential decay fit (line). The pump excitation intensities are the same. The inset is a zoomed-in view marked by the dashed rectangular area. (b) Zoomed-in view of the rising part of the transient THz signal in figure (a). (c) THz responses of the electron-hole plasma, exciton and long-lived state (mid-gap state). (d) Schematic energy diagram of exciton decay dynamics.

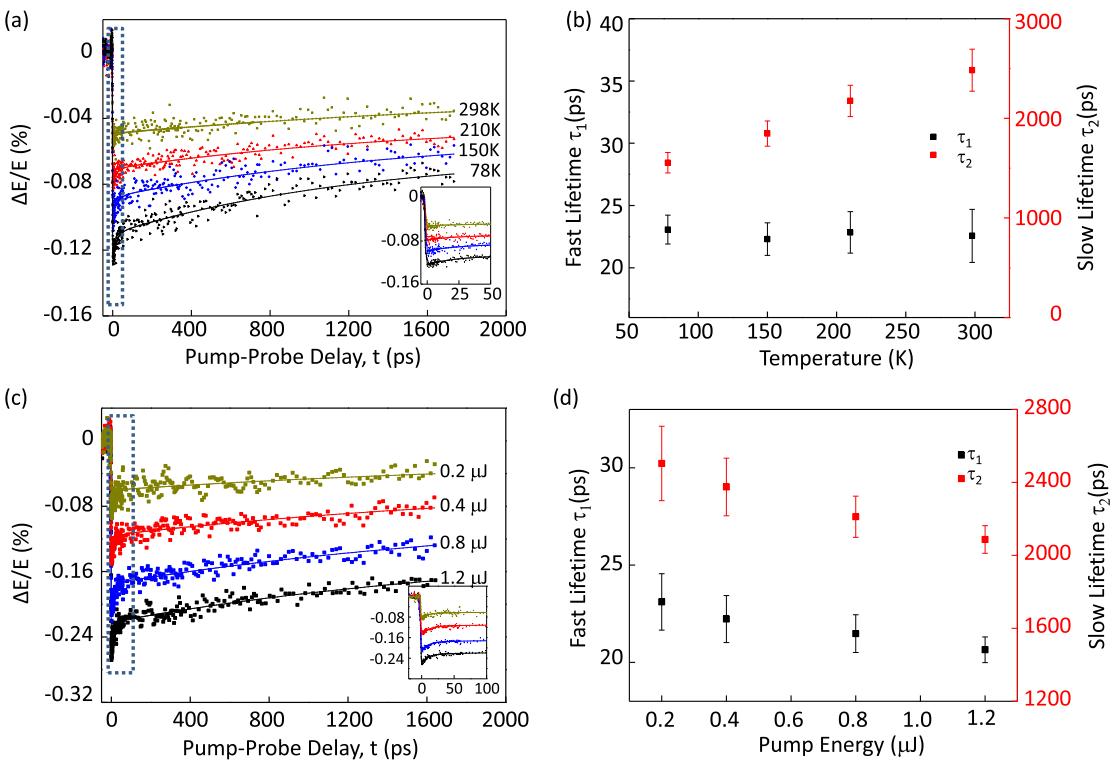

Figure 4. Temperature and pump fluence dependence of the terahertz response. (a) Temporal evolution of transient THz responses of monolayer MoS_2 at 78 K, 150 K, 210 K and 298 K, experimental data (dots) and bi-exponential fit (solid line). The pump excitation is 400 nm with 0.32 μJ energy. The inset is a zoomed-in view of the fast components. (b) Temperature dependence of τ_1 and τ_2 of monolayer MoS_2. (c) Temporal evolution of the transient THz of monolayer MoS_2 with 0.2 μJ, 0.4 μJ, 0.8 μJ and 1.2 μJ pump energy (800 nm) focusing on a 2 mm diameter spot. The inset is a zoomed-in view of the fast decay component. (d) Pump pulse energy dependence of τ_1 and τ_2 of monolayer MoS_2.

10 μJ cm^{-2}. Compared to the 0.124% of ΔE(t, 0)/E(0) in one-photon excitation, the ΔE(t, 0)/E(0) signal is reduced to 0.086% in two-photon excitation. The amplitude of the transient THz signal at time zero does not increase linearly with the excitation density when switching the pump wavelength from 400 nm to 800 nm. This is consistent with the pump-fluence-dependent measurement shown in figure 4(c): the ΔE (t, 0)/E(0) shows saturated behavior (not linear dependence) as a function of excitation carrier intensities. On the other hand, this is also possibly due to many-body effects during the initial stage, which causes different responses in two-photon (800 nm) and one-photon (400 nm) excitation. To fit these data to exponential decays would require at least two exponential terms: a fast component τ_1 and a slow component τ_2. Both components are faster in the bulk than in the monolayer. The temperature dependence of τ_1 and τ_2 is shown in figures 4(a) and (b); while τ_2 increases as the temperature increases, τ_1 is relatively inert regarding temperature in both samples. For pump-fluence-dependent measurements (figures 4(c) and (d), with an 800 nm pump only, due to the limited available pump fluence of 400 nm), both τ_1 and τ_2 decrease as the pump fluence increases. Additionally, the pump fluence dependence of τ_2 in figure 4(d) is also consistent with shorter τ_2 in one-photon excitation (larger excited carrier density) compared to that of the two-photon excitation shown in figure 3(a).

Discussion

Now we turn to the interpretation of the transient THz transmission signal and the related decay dynamics observed in the experiment. The responses of the THz photon to bound and unbound electron-hole states are shown schematically in figure 3(c). The THz response of free carriers (process I), whether from dopants or photo-excitation, can essentially be understood as the charge carriers driven by the alternating electric field of the THz. The initial negative differential THz transmission signal around time zero can be explained by the free carrier absorption of THz due to the photo-excitation of the electron-hole plasma by the pump pulse. However, an attempt to fit the conductivity of the monolayer with a pure Drude model either before or at different delays after pump excitation fails—as shown in the supplementary materials—indicating that the THz response is not purely dominated by free carriers, even before pump excitation. Many factors can contribute to the failure of the standard Drude model, such as tunneling transport through the grain boundary beyond the pure free carrier response, the low initial doping intensity without pump excitation [38, 39], and the effect of lateral diffusion/transport occuring in the area with the pump beam but without the probe beam [40]. The dominating mechanism still remains elusive. After photo-excitation, the excited hot electron-hole plasma relaxes and forms the exciton very rapidly. As the clear exponential decay component cannot be resolved in the initial stage, it suggests that the exciton formation time is shorter than the THz pulse (~1 ps). The fast exciton formation time is expected as the binding energy is extremely large due to reduced screening. Because the exciton is neutral, the terahertz field only couples weakly to the exciton through non-resonant interaction: the polarizability associated with the electron and hole wavefunctions of the exciton. We note that no resonant absorption peak is observed in the THz transmission spectrum after pump excitation (supplementary materials), showing no resonant absorption due to intra-excitonic transitions [20] in the few THz range. This is consistent with the large amounts of exciton binding energy in MoS_2. Additionally, this coupling can be further modified if the exciton is localized by the trapping center or scattering between different exciton species; for example, a mid-gap dark state (process III in figure 1(b) and figure 3(c)).

In figure 3(d), we have constructed a three-level model to account for the bi-exponential decay dynamics in the transient THz measurement. $|0$ is the vacuum state, $|X$ is the exciton state, and $|L$ is the long-lived state. We denote the total radiative and non-radiative decay rate of the exciton $|X$ (long-lived state$|L$) to $|0$ as Γ (Γ_L). On the other hand, $|X$ can relax to $|L$ with the decay rate Γ_1, and $|L$ can be excited to $|X$ with the rate Γ_2 through scattering with impurities, other excitons or phonons. We assume that THz absorption is proportional to the weighted sum of the $|X$ and $|L$ populations: $\propto n_X + \alpha n_L$, here α accounts for the different responses of the THz to the $|X$ and $|L$ states. The dynamics of the exciton population n_X and the long-lived state population n_L are described by the rate equations:

$$\frac{dn_X}{dt} = -(\Gamma + \Gamma_1)n_X + \Gamma_2 n_L,$$
$$\frac{dn_L}{dt} = \Gamma_1 n_X - (\Gamma_L + \Gamma_2)n_L.$$

The solutions are bi-exponential decay functions: $n_X(t) = Ae^{-t/\tau_1} + Be^{-t/\tau_2}$, $n_L(t) = A'e^{-t/\tau_1} + B'e^{-t/\tau_2}$, where the decay constants are:

$$\tau_1^{-1} \equiv \frac{\Gamma + \Gamma_1 + \Gamma_2 + \Gamma_L + \sqrt{(\Gamma + \Gamma_1 + \Gamma_2 + \Gamma_L)^2 - 4\Gamma\Gamma_2 - 4\Gamma_L(\Gamma + \Gamma_1)}}{2},$$
$$\tau_2^{-1} \equiv \frac{\Gamma + \Gamma_1 + \Gamma_2 + \Gamma_L - \sqrt{(\Gamma + \Gamma_1 + \Gamma_2 + \Gamma_L)^2 - 4\Gamma\Gamma_2 - 4\Gamma_L(\Gamma + \Gamma_1)}}{2}$$

The experimentally observed two exponential decays indicate $\tau_1^{-1} \gg \tau_2^{-1}$, which implies $(\Gamma + \Gamma_1 + \Gamma_2 + \Gamma_L)^2 \gg 4\Gamma\Gamma_2 + 4\Gamma_L(\Gamma + \Gamma_1)$, so we can approximately write $\tau_1^{-1} \approx \Gamma + \Gamma_1 + \Gamma_2 + \Gamma_L$ and $\tau_2^{-1} \approx \frac{\Gamma\Gamma_2 + \Gamma_L(\Gamma + \Gamma_1)}{\Gamma + \Gamma_1 + \Gamma_2 + \Gamma_L}$. The THz absorption is then expected to show a bi-exponential decay:

$\propto n_X + \alpha n_L = (A + \alpha A')e^{-t/\tau_1} + (B + \alpha B')e^{-t/\tau_2}$, with τ_1 the fast lifetime and τ_2 the slow lifetime.

In MoS_2 we expect the decay rate of $|X$ to be much faster than the long-lived state $|L$, that is, $\Gamma \gg \Gamma_L$. Under these limits: $\tau_1^{-1} \approx \Gamma + \Gamma_1 + \Gamma_2$, $\tau_2^{-1} \approx \frac{\Gamma\Gamma_2}{\Gamma + \Gamma_1 + \Gamma_2} + \Gamma_L$. So, τ_1 is determined by the total decay rate of the $|X$ and $|L$ states, τ_2 is given by the sum of the long-lived state decay rate Γ_L and some fraction of Γ_2. Recent measurements have reported exciton lifetimes ranging from sub-ps to ~50 ps [29, 41–43]; however, considering the differences in sample species, defect density, substrate materials (SiO_2, BN versus sapphire substrate) and experimental temperature, the measured 20 ps lifetime with the THz probe is within reasonable range. Additionally, τ_1 decreases as pump fluence increases (figure 4(d)), indicating an exciton–exciton annihilation process [14, 44] under experimental excitation conditions. In both the monolayer and bulk MoS_2, τ_1 shows a very weak lattice temperature dependence (figure 3 and figure S3). Theoretically, the temperature dependence of τ_1^{-1} is determined by several terms together. When the temperature increases, the effective radiative lifetime of $|X$ gets longer (Γ decreases) [45], while both Γ_1 and Γ_2 becomes larger as they involve phonon scattering. Using $\tau_1^{-1} \approx \Gamma + \Gamma_1 + \Gamma_2$, the temperature dependence of each term may compensate each other, so the dependence of τ_1^{-1} on temperature is inert, as observed in the experiment.

The decay of transient THz response slows down significantly and follows another exponential decay with a lifetime τ_2 on the order of nanoseconds in the monolayer. In MoS_2, the well-studied exciton decay channel is a trapped exciton state (exciton captured by defect states) in the natural exfoliated sample with a large defect density. The trapped exciton emission lifetime has been measured to be 125 ps at 4 K, but disappears at a slightly elevated temperature in time-resolved photoluminescence experiments [22]. However, the experimentally measured τ_2 is an order of magnitude larger, although this discrepancy can be reduced due to a higher measurement temperature (τ_2 increases as temperature increases) and lower excitation density (τ_2 decreases as pump fluence increases). Considering the discrepancy between τ_2 and the previously reported 125 ps trapped exciton lifetime at 4 K [22], we proposed a more probable decay path through a long-lived state (figure 1(b)) that was recently resolved in a population pulsation resonances experiment [46], whose nature was close to a dark exciton state possibly corresponding to forbidden exciton transition. The lifetime of this long-lived state is measured to be 6.3 ns in monolayer $MoSe_2$, and decreases as excitation intensity increases due to the influence of the interaction effects of the exciton (such as exciton–exciton annihilation), which matches our pump-fluence-dependent measurement (figures 4(c) and (d)). While the exact nature of this long-lived state is unknown, possible candidates could be a mid-gap exciton state or an intervalley (K and K′) dark exciton state, as marked in figure 1(b). While the mid-gap state has lower energy than the bright exciton state, the intervalley dark exciton state has only slightly lower energy than the bright exciton state as a consequence of the electron-hole exchange interaction and the screened Coulomb interaction [47]. In either case, the measured temperature dependence of τ_2 (τ_2 increases as temperature increases, figures 4(a) and (b)) can be explained through the three-level model: as temperature increases, the effective radiative decay rate of the bright exciton decreases [45] (thus the total decay rate Γ decreases), so $\tau_2^{-1} \approx \frac{\Gamma\Gamma_2}{\Gamma + \Gamma_1 + \Gamma_2} + \Gamma_L \approx \Gamma\Gamma_2\tau_1 + \Gamma_L$ also decreases. Meanwhile, the change of Γ_2 due to temperature could be insignificant as the temperature excitation either cannot overcome the large energy offset between $|X$ and $|L$ for the mid-gap state, or enhance the intervalley scattering for the intervalley exciton state.

Another process that could also contribute to transient THz recovery during the fast decay process is the formation of a trion state. Trion formation has been discussed extensively in a recent parallel transient THz measurement on a sample with a doping intensity of an order of magnitude larger [1]. A trion state dulls the response to THz due to its increased effective mass compared to free carriers, thus increasing the THz transmission. However, with initial low doping intensity, only a very small portion of the exciton can further bind to an electron to form a trion in our sample, which may account for the opposite transient THz sign to the reference [1]. However, the doping difference does not completely reconcile the discrepancy between the different decay time constants measured in this paper and reference [1]. Considering the almost instantaneous trion formation time required in the trion model and lack of information on grain size, tunneling transport through the grain boundary may account for the main experimental feature in the reference instead of trion formation—especially when the grain size of the sample is small [1]. During the peer review process of this work, we noticed another parallel transient THz work on MoS_2 and WSe_2 with an even higher initial doping intensity, with the THz response mainly being attributed to charge trapping at the surface states in this research [37].

Conclusions

In summary, we have studied the exciton formation and decay dynamics of photo-excited electron-hole plasma through a transient THz measurement. Different bound and unbound phases of photo-excited electron-hole states that are sensitive to the THz field can be resolved clearly in our measurement with two decay components in the monolayer MoS_2: a fast component (~20 ps) attributed to the exciton lifetime, and a slow component (~ns) attributed to the

intermediate mid-gap trapped or dark exciton state. We expect similar dynamics to apply to other monolayer TMDCs due to similarities in their bandstructure and exciton properties. The measured time-resolved evolution of photo-excited carriers enriches our understanding of the basic optoelectronic properties of 2D TMDC and provides new opportunities for developing novel optoelectronic and excitonic devices based on this material.

Acknowledgments

The authors want to acknowledge Xiaodong Xu for helpful discussions. This project has been supported by the National Basic Research Program of China (973 grant nos. 2012CB921300,2014CB920900, 2013CB932603, 2011CB921903, 2012CB921404, 2012CB933404 and 2011CB933003), the National Natural Science Foundation of China (NSFC grant nos. 11274015, 51222201, 51290272, 11304053, 51121091), the Recruitment Program of Global Experts, the Specialized Research Fund for the Doctoral Program of Higher Education of China (grant no. 20120001110066) and the Beijing Natural Science Foundation (grant no. 4142024).

References

[1] Lui C H, Frenzel A J, Pilon D V, Lee Y H, Ling X, Akselrod G M, Kong J and Gedik N 2014 *Phys. Rev. Lett.* **113** 166801
[2] Geim A K and Grigorieva I V 2013 *Nature* **499** 419
[3] Mak K F, He K, Lee C, Lee G H, Hone J, Heinz T F and Shan J 2013 *Nat. Mater.* **12** 207
[4] Mak K F, Lee C, Hone J, Shan J and Heinz T F 2010 *Rev. Lett.* **105** 136805
[5] Splendiani A, Sun L, Zhang Y, Li T, Kim J, Chim C-Y, Galli G and Wang F 2010 *Nano Lett.* **10** 1271
[6] Xu X, Yao W, Xiao D and Heinz T F 2014 *Nat. Phys.* **10** 343
[7] Ross J S *et al* 2013 *Nat. Commun.* **4** 1474
[8] Miller R C and Kleinman D A 1985 *J. Lumin.* **30** 520
[9] Cheiwchanchamnangij T and Lambrecht W R L 2012 *Phys. Rev.* B **85** 205302
[10] Ramasubramaniam A 2012 *Phys. Rev.* B **86** 115409
[11] Chernikov A, Berkelbach T C, Hill H M, Rigosi A, Li Y, Aslan O B, Reichman D R, Hybertsen M S and Heinz T F 2014 *Phys. Rev. Lett.* **113** 076802
[12] Ugeda M M, Bradley A J, Shi S-F, Felipe H, Zhang Y, Qiu D Y, Ruan W, Mo S-K, Hussain Z and Shen Z-X 2014 *Nat. Mater.* **13** 1091
[13] He K, Kumar N, Zhao L, Wang Z, Mak K F, Zhao H and Shan J 2014 *Phys. Rev. Lett.* **113** 026803
[14] Zhu B, Chen X and Cui X 2015 *Sci. Rep.* **5** 9218
[15] Zhang C, Johnson A, Hsu C-L, Li L-J and Shih C-K 2014 *Nano Lett.* **14** 2443
[16] Ye Z, Cao T, O'Brien K, Zhu H, Yin X, Wang Y, Louie S G and Zhang X 2014 *Nature* **513** 214
[17] Berkelbach T C, Hybertsen M S and Reichman D R 2013 *Phys. Rev.* B **88** 045318
[18] Fortin E and Raga F 1975 *Phys. Rev.* B **11** 905
[19] Ulbricht R, Hendry E, Shan J, Heinz T F and Bonn M 2011 *Rev. Mod. Phys.* **83** 543
[20] Kaindl R A, Carnahan M A, Hagele D, Lovenich R and Chemla D S 2003 *Nature* **423** 734
[21] Korn T, Heydrich S, Hirmer M, Schmutzler J and Schüller C 2011 *Appl. Phys. Lett.* **99** 102109
[22] Lagarde D, Bouet L, Marie X, Zhu C R, Liu B L, Amand T, Tan P H and Urbaszek B 2014 *Phys. Rev. Lett.* **112** 047401
[23] Wang R, Ruzicka B A, Kumar N, Bellus M Z, Chiu H-Y and Zhao H 2012 *Phys. Rev.* B **86** 045406
[24] Shi H, Yan R, Bertolazzi S, Brivio J, Gao B, Kis A, Jena D, Xing H G and Huang L 2013 *ACS Nano* **7** 1072
[25] Wang Q, Ge S, Li X, Qiu J, Ji Y, Feng J and Sun D 2013 *ACS Nano* **7** 11087
[26] Kumar N, He J, He D, Wang Y and Zhao H 2014 *Nanoscale* **6** 12690
[27] Mai C, Barrette A, Yu Y, Semenov Y G, Kim K W, Cao L and Gundogdu K 2014 *Nano Lett.* **14** 202
[28] Nie Z, Long R, Sun L, Huang C-C, Zhang J, Xiong Q, Hewak D W, Shen Z, Prezhdo O V and Loh Z-H 2014 *ACS Nano* **8** 10931
[29] Wang G, Bouet L, Lagarde D, Vidal M, Balocchi A, Amand T, Marie X and Urbaszek B 2014 *Phys. Rev.* B **90** 075413
[30] Wang G, Marie X, Gerber I, Amand T, Lagarde D, Bouet L, Vidal M, Balocchi A and Urbaszek B 2015 *Phys. Rev. Lett.* **114** 097403
[31] Sie E J, Frenzel A J, Lee Y-H, Kong J and Gedik N 2015 *Phys. Rev.* B **92** 125417
[32] Zhu C R, Zhang K, Glazov M, Urbaszek B, Amand T, Ji Z W, Liu B L and Marie X 2014 *Phys. Rev.* B **90** 161302
[33] Norris T B 1992 *Opt. Lett.* **17** 1009
[34] Gallot G and Grischkowsky D 1999 *J. Opt. Soc. Am.* B **16** 1204
[35] Ji Q *et al* 2013 *Nano Lett.* **13** 3870
[36] Shimakawa K, Itoh T, Naito H and Kasap S 2012 *Phy. Stat. Sol.* C **9** 2602
[37] Carvalho A, Ribeiro R M and Castro Neto A H 2013 *Phys. Rev.* B **88** 115205
[38] Jeon T-I and Grischkowsky D 1997 *Phys. Rev. Lett.* **78** 1106
[39] Jeon T-I and Grischkowsky D 1998 *Appl. Phys. Lett.* **72** 2259
[40] Tsoy E N and de Sterke C M 2006 *JOSA* B **23** 2425
[41] Moody G *et al* 2015 *Nat. Commun.* **4** 8315
[42] Wang H, Zhang C, Chan W, Manolatou C, Tiwari S and Rana F 2014 arXiv:1409.3996
[43] Mak K F, He K, Shan J and Heinz T F 2012 *Nat. Nanotechnol.* **7** 494
[44] Mouri S, Miyauchi Y, Toh M, Zhao W, Eda G and Matsuda K 2014 *Phys. Rev.* B **90** 155449
[45] Palummo M, Bernardi M and Grossman J C 2015 *Nano Lett.* **15** 2794
[46] Schaibley J R *et al* 2015 *Phys. Rev. Lett.* **114** 137402
[47] Qiu D, Cao T and Louie S G 2015 *Phys. Rev. Lett.* **115** 176801